

Phonon relaxation processes in crystals (NaNO_3) at high pressure and low temperature

M. Jordan, A. Schuch, R. Righini,^{a)} G. F. Signorini,^{b)} and H.-J. Jodl
Universität Kaiserslautern, Fachbereich Physik, Erwin-Schrödinger-Strasse, D-67663 Kaiserslautern, Germany

(Received 22 March 1994; accepted 9 May 1994)

NaNO_3 is investigated in a diamond anvil cell in the pressure range of 0–9 GPa at 21 and 142 K by means of high-resolution Raman spectroscopy (HRRS). The pressure dependent linewidth of ν_1 (symmetric stretch) is determined and discussed in the framework of anharmonic lattice dynamics. The main relaxation pathways are depopulation processes which are influenced by anharmonic terms in the expansion of the crystal potential and by multiphonon densities of states. The interpretation is supported by numerical calculation of multiphonon densities of states.

INTRODUCTION

Phonon relaxation processes are responsible for the finite lifetime and nonzero linewidths of phonon states; they can be described on the basis of the anharmonic expansion of the crystal potential. Studying these processes in the frequency domain, by means of high-resolution Raman spectroscopy (HRRS) and of Fourier transform infrared spectroscopy (FTIR), or in the time domain, by coherent anti-Stokes Raman spectroscopy (CARS) provides basic information on the phonon–phonon coupling mechanism, and is of growing importance for developing and testing model potentials for molecular or ionic crystals.^{1–3} During the past decades, in the great majority of the experiments on this subject special attention has been devoted to the temperature dependence of the linewidths, since different behaviors with temperature are characteristic of different relaxation processes. Much less attention has been paid to a second important parameter that can be varied, i.e., to the external pressure. Temperature and pressure can be considered as two somehow complementary parameters. In fact, in addition to the consequences of the thermal expansion, in most cases the main effect of rising the temperature is that of increasing the population of phonons and, as a consequence, of increasing the efficiency of the relaxation mechanisms and of making the high order processes more probable. On the other hand, the most relevant effect of applying high pressure on a crystal is that of drastically modifying its phonon density of states (DOS). Changing pressure modifies the intermolecular distances (of about 10% going from 0 to 10 GPa), what has considerable influence on the crystal potential and, consequently, on the frequency distribution of phonons and on the anharmonic coupling constants. Measuring linewidths at high pressure and low temperature is quite a new type of experiment, that up to now has been performed successfully on carbon disulfide,^{4–7} carbon dioxide,⁸ and naphthalene.⁹

In Ref. 10 the authors reported quite an unusual behavior with temperature of the linewidth of the ν_1 symmetric stretching vibron observed in sodium nitrate crystal. Be-

tween 0 and 70 K, and above 140 K, the linewidth of this mode increases normally with the temperature, whereas in the intermediate temperature range the linewidth decreases from 0.75 to 0.55 cm^{-1} . This strange behavior was explained as the result of the thermal expansion and of the peculiar density of vibrational states of this crystal. At low temperature in fact the frequency of the ν_1 mode is almost exactly coincident with the sum frequency of ν_2 (NO_3^- bending) plus the Na^+ translational phonons, whose frequencies are almost degenerate with a mean value of about 220 cm^{-1} . The resulting very high and narrow-peaked two-phonon density of states provides a large number of decay channels to ν_1 ; when the temperature rises the thermal expansion of the crystal lowers the frequency of the translational peak, thus reducing the density of two-phonon states resonant with ν_1 . Below 140 K this reduction overcompensates the increase of the phonon thermal population, and the net result is a decrease of the linewidth with increasing temperature. For $T > 140$ K higher order processes, involving different phonon states, become dominant, and the “normal” behavior (i.e., increase of the linewidth with increasing temperature) is recovered. This picture is confirmed by the IR spectra of the phonon sideband of the ν_2 mode, from which the number of final states available for the relaxation of ν_1 can be estimated by considering the absorbance at the frequency corresponding to the IR inactive ν_1 mode. Polarized IR spectra in this region at 80 K, 293 K, and higher temperatures have already been published;¹¹ we have repeated unpolarized measurements at several temperatures below room temperature with a FTIR spectrometer. The spectra at five different temperatures are shown in Fig. 1.

The basic idea of the experiment described here is to measure the linewidth of ν_1 as a function of pressure and temperature that can be varied separately. In such a way it is possible not only to modify to a large extent the DOS, but also to distinguish, among the different parameters which determine the phonon linewidths, temperature effects from volume effects. Our experimental work was paralleled by lattice dynamics calculations, whose contribution was important for a more convincing interpretation of the data. Finally, as a test of the overall picture, similar experiments were performed on KNO_3 , a crystal with almost identical intramo-

^{a)}LENS (European Laboratory for Nonlinear Spectroscopy), University of Florence, Largo Enrico Fermi 2, I 50125, Firenze, Italy.

^{b)}Department of Chemistry, University of Florence, via G. Capponi, I 50121, Firenze, Italy.

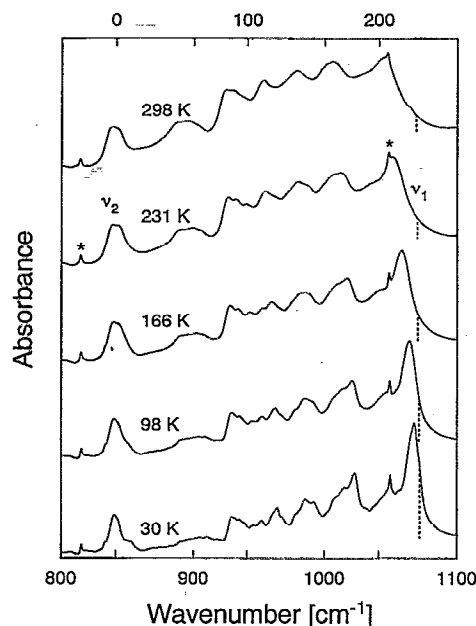


FIG. 1. FTIR spectra of the ν_2 mode and its sideband of NaNO_3 at $p=0$ and several temperatures. The position of the IR inactive mode ν_1 is indicated by the line near 1070 cm^{-1} . The length of the ν_1 marker is a measure for the DOS. The upper scale is wave numbers relative to the ZPL. The two features indicated by an asterisk are due to ν_1 and ν_2 modes of isotopic impurities.

lecular vibrational frequencies, whose DOS is quite different, due to the larger mass of the cations.

THEORETICAL BACKGROUND

Line broadening mechanisms can be classified as homogeneous and inhomogeneous broadening. The former one arises from anharmonicity and exhibits a pure Lorentzian line shape, whereas the latter one leading to Gaussian line profiles is due to crystal imperfections such as isotopic impurities or strain, as is the case in real crystals. Inhomogeneous broadening occurring even at low temperature is more difficult to describe mathematically than homogeneous broadening and will not be discussed here. The special case of isotopic impurities is investigated in Ref. 12.

Finite Raman and infrared linewidths originate from anharmonic terms in the expansion of the crystal potential. In the harmonic approximation, phonons are noninteracting quasiparticles having infinitely long lifetimes and therefore delta-shaped line profiles in the corresponding spectra. Anharmonic terms of the crystal potential couple phonons together leading to finite lifetimes, or nonzero linewidths.

In the framework of perturbation theory, the width of a spectral line can be expressed as the sum of an infinite series that converges rapidly if anharmonicity is small;^{1,2} each term in the series represents a class of relaxation processes. Due to energy and momentum conservation requirements, only a limited number of processes can contribute to the width of a given line. As already mentioned, in the case of ν_1 of NaNO_3 the only active relaxation pathways at low temperatures is down conversion to ν_2 plus one or more lattice phonons.

The contribution to the total linewidth of a three-phonon down process $\omega_l \rightarrow \omega_m + \omega_n$ is given by²

$$\Gamma_l^{(3d)}(T) = \frac{36\pi}{\hbar^2} \sum_{m,n} |B_{lmn}|^2 (n_m + n_n + 1) \delta(\omega_l - \omega_m - \omega_n), \quad (1)$$

where B_{lmn} are coupling constants related to the third derivatives of the crystal potential and n_m, n_n are the phonon occupation numbers $\{n_i = [\exp(\hbar\omega_i/kT) - 1]^{-1}\}$ at temperature T . The contribution of a four-phonon down process is

$$\Gamma_l^{(4d)}(T) = \frac{192\pi}{\hbar^2} \sum_{mnp} |B_{lmnp}|^2 ((n_m + 1)(n_n + 1)(n_p + 1) - n_m n_n n_p) \delta(\omega_l - \omega_m - \omega_n - \omega_p). \quad (2)$$

Higher order processes have similar expressions.

If the coefficients $B_{lm\dots}$ do not vary very much over the Brillouin zone they can be replaced by an averaged $\langle B_{lm\dots} \rangle$ and the occupation numbers can be replaced by effective ones such that the sum extends only over the Kronecker delta, i.e., the multiphonon density of states.

In the vicinity of $T=0$, three-phonon down conversion dominates the relaxation of ν_1 (Ref. 10), so the linewidth is essentially given by Eq. (1), which now reads

$$\Gamma_l^{(3d)} \propto \langle B_{lmn} \rangle^2 \rho_{\text{sum}}(\omega_l) n(T), \quad (3)$$

where $\rho_{\text{sum}}(\omega_l)$ is the two-phonon sum density of states and $n(T)$ is an abbreviation for the sum term of the occupation numbers for the corresponding process. This equation is the basis for interpreting linewidth data at zero pressure/varying temperature as well as zero temperature/varying pressure. In the former case $\Gamma(T) \propto n(T)$ because B and ρ can be treated as constant (if thermal expansion is neglected). In many cases this assumption is justified and the temperature dependence of the linewidth can be reproduced only by considering $n(T)$ (e.g., the ν_3 and ν_4 mode in NaNO_3 , Ref. 10) but there are exceptions like ν_1 in NaNO_3 , where at least ρ is strongly temperature dependent. In the second case, where T approaches zero, the phonon occupation numbers vanish and $n(T) = 1$. Therefore the linewidth contribution is simply the product of a mean coupling constant and the associated density of states. These quantities can be calculated for each crystal structure relative to each pressure of interest. If ω_l and ω_m are internal modes with small dispersion (like ν_1 and ν_2) ρ_{sum} is well approximated by the one-phonon DOS at the frequency $\omega_l - \omega_m$:

$$\Gamma_l^{(3d)} \propto \langle B_{lmn} \rangle \rho_1(\omega_l - \omega_m). \quad (4)$$

This equation was used for the calculation of the linewidth at low temperature and for the interpretation of our experimental results.

EXPERIMENT AND RESULTS

In the past NaNO_3 was mainly investigated because of the presence of an order-disorder phase transition beginning at 423 K and reaching the λ point at 549 K.^{13,14} Below this temperature sodium nitrate consists of alternate layers of Na^+ and planar NO_3^- ions perpendicular to the threefold c

axis where the orientation of the nitrate groups in a given layer differs by 60° from the groups in two adjacent nitrate layers.^{15,16} This is the ordered calcite structure D_{3d}^6 or $R\bar{3}c$ with two formula units per primitive cell. Group theory predicts 27 optical modes which can be divided for $k=0$ into external (lattice modes below approximately 300 cm^{-1}) and internal modes originating from the vibrations of the nitrate ion above 725 cm^{-1} .

At temperatures below 384 K KNO_3 is found to be in phase II (D_{2h}^{16}), the orthorhombic aragonite structure with four formula units in the Bravais unit cell.^{17,18}

The experiments were carried out on two single crystals of NaNO_3 (in the figures referred to as No. 1 and No. 2) and one single crystal of KNO_3 , all grown from aqueous solution and of unknown orientation. Their quality (strain, stress) was checked with crossed polarizers. Each crystal was placed in the gasket hole (diameter: $150\text{ }\mu\text{m}$; height: $80\text{ }\mu\text{m}$) of a diamond anvil cell (DAC); furthermore at least two ruby chips (diameter $\leq 20\text{ }\mu\text{m}$) were added serving as manometer. Helium, filled by application of the gas loading technique (initial pressure 0.27 GPa), was used as a pressure transmitting medium because it is the most hydrostatic material known even at low temperature. The DAC was mounted on the cold flange of a closed cycle cryostat which cooled the sample down to approximately 20 K during 6 h (cooling power at 20 K: 7.7 W). Temperature was monitored by two silicon diodes which were placed at the top and bottom of the cell. Their temperature difference was below 3 K giving rise to the assumption that no considerable temperature gradient over the cell is present. Pressure was measured by the well-known ruby fluorescence method with an uncertainty of 0.1 GPa.¹⁹ Pressure was increased exclusively at room temperature because there helium is in its fluid state up to 12 GPa. Therefore we expect no generation of stress during pressure increase.

Raman light was excited by an argon ion laser running in single mode on the 514.5 nm line at 200 mW output power. Due to transmission losses the power at the sample is about 100 mW. Collected Raman light is focused by a lens on a pin hole which serves as a point light source for the subsequent lens generating parallel light. In that region the pressure tuned Fabry-Perot interferometer (FPI) is placed which is the high-resolution element of our setup. Transmitted light is focused by a third lens on the entrance slit of the monochromator which serves as the preselector. Standard photon counting equipment in conjunction with a personal computer was used for recording spectra and interferograms. The FPI was equipped with spacers having 2 and 3 mm thickness corresponding to 2.5 and 1.7 cm^{-1} free spectral range (FSR) and approximately 0.04 and 0.03 cm^{-1} bandpass. This configuration enables us to measure linewidths as small as 0.02 cm^{-1} . A more detailed description can be found in Ref. 5.

Our interest is mainly focused on the pressure dependent linewidth evolution of the ν_1 mode at 1071 cm^{-1} . Nevertheless it was necessary to take at least low-resolution spectra of the lattice region and of the ν_1 mode to determine line positions. Figures 2 and 3 summarize the pressure dependent frequencies at $T=21\text{ K}$ of the two Raman active external modes $E_g(T)$ and $E_g(R)$, where T and R are translation and

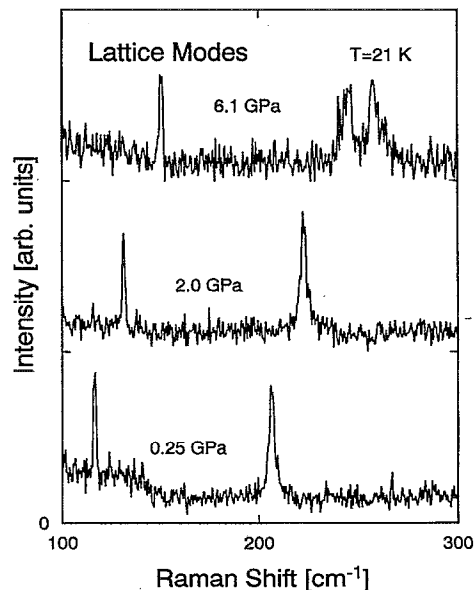


FIG. 2. Raman spectra of the lattice mode region of NaNO_3 at $T=21\text{ K}$ and several pressures.

rotation, respectively. Between 0 and 2 GPa the line position is given by $\nu[E_g(T), p] = 8.6 \cdot p + 116$ and $\nu[E_g(R), p] = 9.4 \cdot p + 205$, where the units are GPa and cm^{-1} . The pressure shift of these two modes serves as a check for the model potential discussed in the next section. Above 6 GPa the $E_g(R)$ mode splits due to a II/III phase transition which was already observed.²⁰

The pressure shift of the internal mode ν_1 is shown in Fig. 4 [empirical fit: $\nu(\nu_1) = 1078.5 + 2.7 \cdot p - 8.4 \cdot \exp(-p/0.79)$; units in GPa and cm^{-1}]. Concerning the Raman forbidden ν_2 mode we refer to Adams *et al.*,²⁰ who have measured the overtone of ν_2 and found a shift of $1.2\text{ cm}^{-1}/\text{GPa}$. If no unusual pressure dependence of ν_2 and its

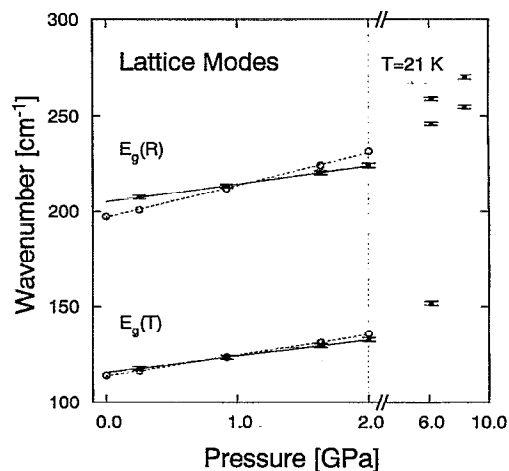


FIG. 3. Pressure dependence of observed (solid circles with error bars, $T=21\text{ K}$) and calculated (open circles, $T=0\text{ K}$) lattice mode frequencies of NaNO_3 . The solid and dotted lines serve as a guide for the eye.

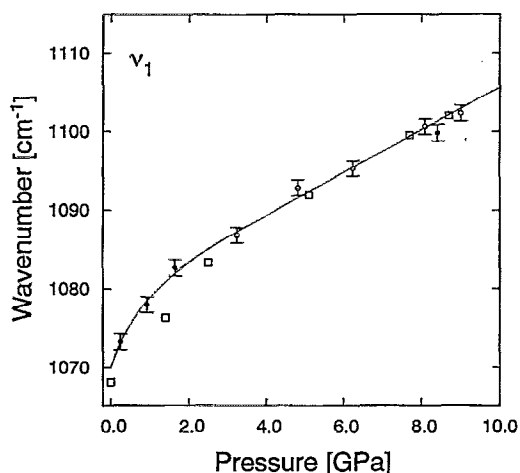


FIG. 4. Pressure dependence of the ν_1 mode of NaNO_3 at $T=21$ K. Open circles with error bar: crystal No. 1; solid circles with error bar: crystal No. 2; \square : Ref. 20 (room temperature). The solid line serves as a guide for the eye.

overtone occurs, the pressure shift of the fundamental is estimated to be $0.6 \text{ cm}^{-1}/\text{GPa}$ which is in any case small compared to the other pressure shifts under discussion. Teo *et al.* (Ref. 21) observed a discontinuity of the line position of ν_1 at approximately 1.6 GPa and the disappearance of the translational lattice mode at slightly lower pressure at room temperature. Neither Adams *et al.*²⁰ nor our group observed a similar behavior; therefore we conclude that below 6 GPa no phase transition occurs at 20 and 140 K.

However the main result is the pressure dependent linewidth of ν_1 at 21 and 142 K which is shown in Figs. 5 and 6. Low and high temperature data are very different: at 20 K linewidth decreases from the zero pressure value of 0.7 cm^{-1}

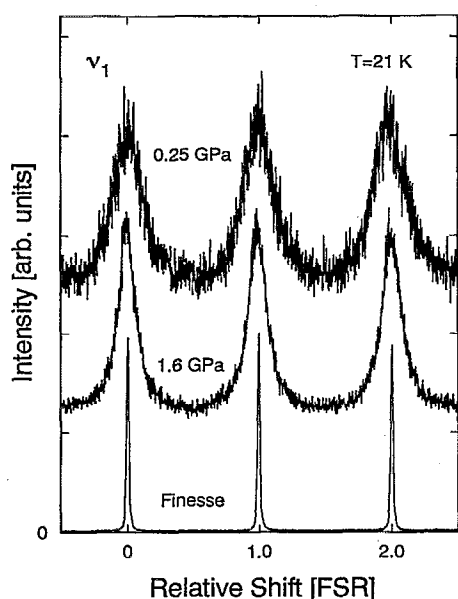


FIG. 5. Interferograms of the ν_1 mode of NaNO_3 at $T=21$ K and several pressures.

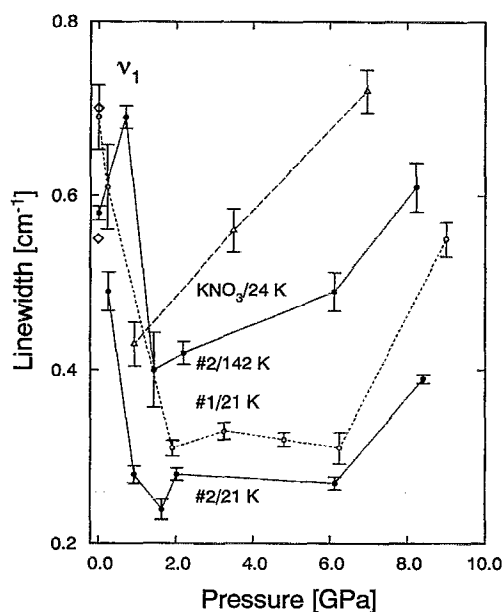


FIG. 6. Pressure dependence of the linewidth of ν_1 of NaNO_3 at 21 and 142 K (open circles: crystal No. 1; solid circles: crystal No. 2) and KNO_3 at $T=24$ K (open triangles); \diamond : Ref. 10.

(Ref. 10) to 0.3 cm^{-1} at 2 GPa, whereas at 140 K the linewidth initially increases from 0.55 cm^{-1} (Ref. 10) at zero pressure to 0.7 cm^{-1} at 1 GPa and decreases to approximately 0.4 cm^{-1} at 2 GPa. The increase of linewidth above 6 GPa is probably due to the II/III phase transition and will not be discussed here. For comparison interferograms of the ν_1 mode of KNO_3 were recorded and linewidth data added to Fig. 6.

Furthermore FTIR spectra in the ν_2 region (zero phonon line+sideband) of a NaNO_3 single crystal at zero pressure and above 30 K were taken to get information on the DOS in the lattice region (Fig. 1). This sideband reproduces at least qualitatively several features of the DOS and in particular the translational peak (see below) of the one-phonon density of states around 225 cm^{-1} . The corresponding zero-phonon line (ZPL) is ν_2 , which is the origin of the sideband. Thus the translational peak is mapped to 1068 cm^{-1} ($=842 \text{ cm}^{-1}+226 \text{ cm}^{-1}$). The DOS is one factor controlling the linewidth [Eq. (3)] and it can be directly estimated from the IR spectra as the absorbance at the frequency of ν_1 . In Fig. 1 the length of the bars is an estimate for the DOS and the position corresponds to the infrared inactive ν_1 mode. However, sidebands are not identical to the DOS but are weighted by a complicated response function.

CRYSTAL MODEL AND CALCULATION

The pressure dependence of the phonon density of states of NaNO_3 crystal was obtained at different temperatures by performing lattice dynamics calculations at the appropriate crystal densities. Since no high pressure/low temperature data about the crystal structure are available, the following extrapolation procedures were applied to calculate $a(p,T)$ and $c(p,T)$ from few experimental data: (1) lattice param-

TABLE I. Model potentials.

Potential parameters (units: kcal/mol and Å)				
$V(r) = A_{ij} \exp(-B_{ij}r) - C_{ij}r^{-6}$				
<i>i</i>	<i>j</i>	A_{ij}	B_{ij}	C_{ij}
Na	Na	9 601	3.15	24.2
Na	N	20 096	3.46	79.2
Na	O	22 529	3.72	64.2
N	N	42 065	3.78	259.1
N	O	57 162	3.98	259.2
O	O	76 054	3.67	197.8
Charges (units: proton charge)				
<i>i</i>				q_i
Na				1.000
N				0.098
O				-0.366

eters at ordinary pressure (0 GPa) and 0 K were obtained using structure data at room temperature¹⁶ and thermal expansion data between 80 K and room temperature;²² (2) an empirical $p(V)$ relationship, based on room temperature data below 2.5 GPa,²³ was extended to low temperatures using the 0 K, 0 GPa structure, considering a general state equation for the crystal;²⁴ 3. the a/c ratio was assumed to depend linearly on pressure and to be independent of T . The same procedure was applied to $T = 140$ K. In this way, the following expressions for the lattice parameters were obtained (units of Å and GPa):

$$a(p, T=0 \text{ K}) = 5.061 - 0.0325 \cdot p, \quad (5a)$$

$$c(p, T=0 \text{ K}) = 16.502 - 0.330 \cdot p, \quad (5b)$$

$$a(p, T=140 \text{ K}) = 5.062 - 0.0323 \cdot p, \quad (5c)$$

$$c(p, T=140 \text{ K}) = 16.582 - 0.330 \cdot p. \quad (5d)$$

Finally, the N–O distance was assumed to be constant (the positions of Na^+ and N and the orientation of the NO_3^- ion are fixed by symmetry).

It must be emphasized that the crystal structures obtained with this procedure cannot be regarded as “experimental.” However, since they reproduce to a reasonable degree of accuracy the effects of pressure, they were used as starting points for our model calculations. The interionic potential we employed consists of an atom–atom interaction in the “6-exp form” plus a point-charge model. Initial values for the parameters were taken from molecular dynamics simulations of NaNO_2 crystals²⁵ and of the Ca/K/NO_3 melt.²⁶

TABLE III. Calculated and experimental lattice mode frequencies of NaNO_3 at zero pressure.

Symmetry	Calc., $T=0$	Expt. (Ref. 31) $T=10 \text{ K}$	Expt. (this work)
			$T=21 \text{ K}$, extrapolated to $p=0$
A_{1u}	214.6		
A_{2g}	228.7		
A_{2g}	160.8		
E_g	197.3		205.5
E_g	114.1		115.7
A_{2u} (TO)	225.4	223.0	
A_{2u} (TO)	56.6	55.0	
A_{2u} (LO)	298.3	290.1	
A_{2u} (LO)	114.2	121.2	
E_u (TO)	220.6	223.0	
E_u (TO)	182.9	182.0	
E_u (TO)	85.2	90.0	
E_u (LO)	295.5	257.5	
E_u (LO)	195.4	198.0	
E_u (LO)	109.3	102.0	

A refinement of the potential parameters A_{ij} , B_{ij} , C_{ij} , and q_i , based on the extrapolated crystal structures and on the experimental data for the lattice energy and optical phonon frequencies at different pressures (when available), led to the set given in Table I. A good fit to the data is reached mainly through a hardening of the O–O interaction with respect to the starting potential. This partly compensates for the lack of polarizability contributions.

One cell parameter (a) is reproduced correctly, while the other (c) is larger than its extrapolated counterpart by about 15% (see Table II). As shown in Table III, the agreement for lattice mode frequencies at $p=0$ is satisfactory. The pressure dependence of some lattice phonons is illustrated in Fig. 3: the frequency variation is nearly correct for the lower (translational) mode, while it is about two times the experimental value for the higher (rotational) mode. LO frequencies are also too high. As usual in similar calculations on ionic systems, the potential results too “stiff” if polarizability is not taken into account. However, including polarizability, e.g., through a shell model, implies the use of extra parameters that would make the refinement process much more complicated. In view of the approximations implicit in the model (e.g., the approximations on crystal structures at high pressure—see above) no effort was made to go beyond the rigid ion approximation.

As already pointed out, the phonon density of states is

TABLE II. Calculated and extrapolated [Eqs. (5a) and (5b)] lattice constants and calculated lattice energy of NaNO_3 at $T=0$.

p (GPa)	a (Å)		c (Å)		Lattice energy (kcal/mol)	
	Calculated	Extrapolated	Calculated	Extrapolated	Calculated	(Ref. 30)
0.0	5.004	5.061	19.071	16.502	-165.060	-182.934
0.24	4.993	5.053	18.957	16.423		
0.92	4.966	5.031	18.666	16.198		
1.63	4.942	5.008	18.401	15.964		
2.03	4.930	4.995	18.265	15.832		

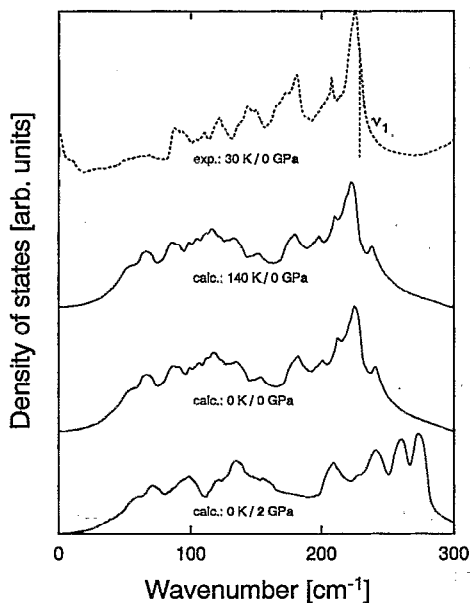


FIG. 7. Calculated one-phonon density of states (DOS) of the lattice mode region of NaNO_3 . The area under the calculated curves is normalized to 1. For comparison the phonon sideband of ν_2 is shown (broken line), where the first moment of this fundamental ν_2 is taken as the zero-phonon line.

the quantity of interest in the calculation of the relaxation probability of ν_1 . Densities of states were calculated at different pressures by sampling about 10 000 points uniformly distributed in the Brillouin zone of the appropriate crystals. The calculation was made for $T=0$ and 140 K using the corresponding crystal structures; some results are shown in Fig. 7. These curves can be compared to the phonon sideband observed in the ν_2 region of the infrared spectrum, which shows a similar peak structure, although it should be kept in mind that the intensity of the IR profile is not simply proportional to the phonon DOS, but is weighted by a response factor depending on frequency. Figure 7 shows the dependence of the DOS on p and T , which is in the expected direction, even though the temperature shift appears to be smaller than in the experiments. This shows that while the potential curve is somehow too steep on the side of the short distances (experienced by the crystal at high pressures), on the long distance side (corresponding to higher temperatures) it is probably too flat.

In Fig. 8, the phonon DOS around the resonance frequency ($\nu_1 - \nu_2$) is plotted vs. pressure in the interval 0–2 GPa, which is the range of validity of crystal structure extrapolations and of the fitting of vibrational frequencies. The curves represent the average value of the DOS at $225 \pm 5 \text{ cm}^{-1}$. This interval (10 cm^{-1}) corresponds to the dispersion of the ν_2 band,²⁷ and also takes care of the uncertainty about the pressure dependence of this mode. An initial, steep decrease with pressure is calculated at $T=0$ K, while the curve at $T=140$ K shows a small plateau at low pressures. This behavior qualitatively reproduces the pressure dependence of ν_1 linewidth (see Fig. 6).

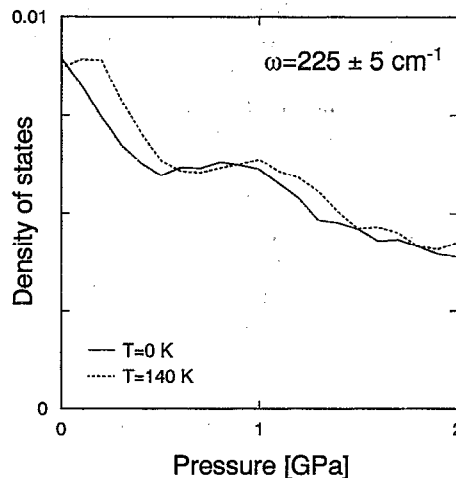


FIG. 8. Calculated phonon DOS of NaNO_3 around $\omega=225 \text{ cm}^{-1}$ at 0 and 140 K. The scale is the fraction of the integrated phonon density of states.

DISCUSSION

As was anticipated in the Introduction, the unusual quality of sodium nitrate is a peak in the one-phonon density of states at approximately 225 cm^{-1} (in the following called simply “translational peak”) originating from the translational motion of the Na^+ ion against the NO_3^- ion which nearly equals the difference in wave number of ν_1 (1071 cm^{-1}) and ν_2 (842 cm^{-1}). Therefore a three-phonon down process ν_1 (1071 cm^{-1}) \rightarrow ν_2 (842 cm^{-1}) + ω_L (229 cm^{-1}) with many final states and consequently large linewidth is likely to exist. This can be seen in the FTIR spectrum of Fig. 1 where the ν_1 position is marked by the line around 1070 cm^{-1} and the estimated number of available final states is indicated by the length of that line (see above). As the temperature increases the translational peak shifts to lower frequencies [the temperature dependence can be expressed by the formula $\nu_1 = 1067.9 - 16.2[\exp(160/T) - 1]$ [K, cm^{-1}], which is the common expression for temperature dependent line shift²⁸] whereas the frequencies of the internal modes remain almost constant ($\Delta\nu_1/\Delta T \sim -0.02 \text{ cm}^{-1}/\text{K}$ and $\Delta\nu_2/\Delta T \sim -0.008 \text{ cm}^{-1}/\text{K}$). Therefore the number of final states and consequently the linewidth of ν_1 decreases between 80 and 140 K. Below 80 K the linewidth evolution is in agreement with a three-phonon down process with constant linewidth below 40 K ($\Gamma=0.7 \text{ cm}^{-1}$) and slightly increasing linewidth above 40 K ($\Gamma=0.73 \text{ cm}^{-1}$ at 70 K). The nonlinear temperature dependence of the linewidth above 140 K can be ascribed to contributions from the four-phonon down process: ν_1 (1070 cm^{-1}) \rightarrow ν_2 (842 cm^{-1}) + $2 \times \omega_L$ (114 cm^{-1}). This is the model used by Angeloni and Righini to explain the temperature dependent linewidth evolution of ν_1 (Ref. 10).

The pressure dependent linewidth at low temperature is given by Eq. (4) and depends in this approximation on the averaged coupling coefficient $\langle B_{12L} \rangle$, which is a third derivative of the crystal potential with respect to ν_1 , ν_2 , and a lattice phonon, and the density of states of the lattice modes region.

Since high pressure IR spectroscopy experiments cannot be executed in our laboratory, we have no experimental access to such DOS data. Nevertheless the calculated DOS at the difference frequency of ν_1 and ν_2 as a function of pressure (Fig. 8) qualitatively reproduces the main characteristics of the $\Gamma(p)$ curve in Fig. 6. At $T=0$ K the DOS decreases by 56% between 0 and 2 GPa which is comparable to the decrease of the linewidth in the same pressure range (0.7→0.3 cm^{-1}). As can be seen in Fig. 7 the structure of the DOS above 200 cm^{-1} changes dramatically with pressure and in particular the translational peak loses intensity.

The second factor of Eq. (4), $\langle B_{12L} \rangle$, is expected to be slowly increasing with pressure, as can be seen by the following consideration. Unfortunately, it is difficult to calculate this quantity “*a priori*,” due to the lack of information about high-order derivatives involving the internal potential of NO_3^- , which is part of the crystal potential. However, one can estimate the pressure variation of $\langle B_{12L} \rangle$ from that of an average coupling coefficient $\langle B_L \rangle$ involving only external modes: we found that $\langle B_L \rangle$ varies almost linearly with pressure and increases by a factor of about 1.6 in the interval 0–2 GPa. Since the increase in $\langle B_{12L} \rangle$ is probably much smaller than that [the internal potential is less dependent on pressure than the external potential, as shown also by the $\nu(p)$ curves²⁰], we can regard this value as an upper limit. If the balanced effect of the DOS decrease and of the $\langle B_{12L} \rangle$ increase is considered, the overall self-energy change in the same interval results to be at least -27% , a value which is in good agreement with the observed $\Gamma(p)$.

Thus, on the whole, our model indicates that at low T the pressure induced change in the high-frequency region of the DOS is the driving force for the linewidth variation. However, as Fig. 7 shows, the effect of pressure is not merely a rigid shift of the translational peak [since the pressure shift is <1 $\text{cm}^{-1}/\text{GPa}$ for $(\nu_1 - \nu_2)$ and about 10 cm^{-1} for lattice frequencies, this would cause an initial increase of Γ with p], but rather a transformation in its shape.

The same discussion is applicable to the curve at $T=140$ K, in which case, however, the thermal factor $n_L(T=140\text{ K})+1 \approx 1.1$ should also be taken into account [Eq. (3)]. The changes of the coefficients $\langle B_{12L} \rangle$ with temperature are treated to be small compared to pressure induced effects. The main difference to the low-temperature case is the position of the translational peak of the sideband, which is 10 cm^{-1} below ν_1 (Fig. 1). This is the reason for the reduced linewidth (0.55 cm^{-1} , Ref. 10) at zero pressure as already discussed above. Increasing pressure again broadens the translational peak and generates new features in the high-frequency part of the one-phonon DOS (Fig. 7) leading there to increased DOS at 225 cm^{-1} and consequently to the initial increase of linewidth (see Fig. 6). This behavior is reproduced theoretically by the pressure dependent DOS at 225 cm^{-1} at 140 K (Fig. 8).

State densities were not calculated above 2 GPa (as already noted, the extrapolation of lattice parameters is limited to max. 2.5 GPa), but Fig. 8 indicates that no significant difference, between the low T case and the 140 K case, is to be expected above this pressure. Since the thermal factor alone can account for only a fraction (<0.1 cm^{-1}) of the

linewidth difference between the two temperatures in the range 2–6 GPa, higher order phonon relaxation processes must be responsible for the rest of this difference. We calculated that the contribution of four-phonon down conversion approximately doubles in the interval 20–140 K, with $\Gamma^{(4)} \sim 0.2$ cm^{-1} at the higher temperature.¹⁰ This value is in good agreement with our experiments.

Finally we recorded some interferograms of the ν_1 mode of KNO_3 which served as a crosscheck. Linewidth increases from 0.4 cm^{-1} at $p=0$ to 0.7 cm^{-1} at 6 GPa as expected, which is completely different to the linewidth evolution of ν_1 in NaNO_3 (Fig. 6). Since the frequencies of the internal modes, originating from the vibrations of the NO_3^- ion, are almost identical to those of NaNO_3 (KNO_3 at 78 K²⁹: $\nu_1=1054$ cm^{-1} , $\nu_2=827$ cm^{-1}) we expect that differences mainly arise from intermolecular interaction and—of course—from the heavier K^+ ion. Considering only masses, the translational peak is expected at approximately 175 cm^{-1} , which is 50 cm^{-1} lower than in NaNO_3 . IR spectra of the phonon sideband of ν_2 of KNO_3 , which are unfortunately much less structured than in NaNO_3 , exhibit slightly enhanced absorption around 990 cm^{-1} corresponding to a more intense sideband and therefore to a larger DOS at 160 cm^{-1} which is in the expected direction. Raman spectra in the ν_1 region also exhibit phonon sidebands²⁹ whose highest frequency is separated by ≈ 170 cm^{-1} from the fundamental. Moreover, the high-energy tail of the phonon sideband extends up to 1040 cm^{-1} corresponding to a Debye frequency in the lattice region of approximately 210 cm^{-1} . All these findings support the assumption that at $p=0$ GPa no three-phonon down channel is available: ν_1 (1054 cm^{-1})→ ν_2 (827 cm^{-1})+ ω (227 cm^{-1}) because the difference frequency (227 cm^{-1}) is larger than the Debye frequency (210 cm^{-1}); however four-phonon down processes cannot be excluded. At elevated pressure the Debye frequency increases at a rate similar to that of high lying external modes (A_g at 165 cm^{-1} : 8.2 $\text{cm}^{-1}/\text{GPa}$) and a three-phonon down channel may open. This should lead to increasing linewidth of ν_1 in KNO_3 being in accordance with the experimental results.

SUMMARY

High-resolution Raman measurements were executed on NaNO_3 at pressures up to 9 GPa at 21 and 142 K. The abnormal decrease in linewidth is discussed in the framework of anharmonic lattice dynamics considering in particular pressure induced changes of anharmonicity constants and phonon densities of states. In particular the pressure induced change of the shape of the translational peak in the one-phonon density of states in the lattice mode region is responsible for the observed linewidths. Numerical calculations (DOS at several pressures) based on extrapolated lattice parameters reproduce the decrease of linewidth to a reasonable degree. The limiting factor for more precise calculations is again the lack of accurate structure data at low temperature and high pressure.⁵ Additionally, KNO_3 was measured because of the different crystal structure and different masses of the metal ion leading to modified DOS in the lattice region. The result—an almost linear increase of linewidth with

pressure—can be explained by considering a three-phonon down process, whose efficiency increases with pressure due to increased number of final states.

- ¹S. Califano, V. Schettino, and N. Neto, *Lattice Dynamics of Molecular Crystals* (Springer, Berlin, 1981).
- ²S. Califano and V. Schettino, *Int. Rev. Phys. Chem.* **7**, 19 (1988).
- ³P. Foggi and V. Schettino, *Riv. Nuovo Cimento* **15**, No. 7 (1992).
- ⁴M. Jordan, H. Däüfer, and H.-J. Jodl, in *Frontiers of High-Pressure Research*, edited by H. D. Hochheimer and R. D. Ethers (Plenum, New York, 1991).
- ⁵H.-J. Jodl, M. Jordan, and H. Däüfer, *J. Chem. Phys.* **98**, 2332 (1993).
- ⁶E. L. Chronister and R. A. Crowell, *Chem. Phys. Lett.* **182**, 27 (1991).
- ⁷R. A. Crowell and E. L. Chronister, *J. Phys. Chem.* **96**, 1045 (1992).
- ⁸M. Baggen and A. Lagendijk, *Chem. Phys. Lett.* **177**, 361 (1991).
- ⁹R. A. Crowell and E. L. Chronister, *J. Phys. Chem.* **96**, 9660 (1992).
- ¹⁰L. Angeloni and R. Righini, *Chem. Phys. Lett.* **154**, 115 (1989).
- ¹¹S. V. Karpov and A. A. Shultin, *Sov. Phys. Dokl.* **13**, 454 (1968).
- ¹²A. A. Maradudin and S. Califano, *Phys. Rev. B* **48**, 12,628 (1993).
- ¹³M. D. Fontana, F. Brehat, and B. Wyncke, *J. Phys. Condensed Matter* **2**, 9125 (1990).
- ¹⁴H. Yasaka, A. Sakai, and T. Yagi, *J. Phys. Soc. Jpn.* **54**, 3697 (1985).
- ¹⁵P. Cherin, W. C. Hamilton, and B. Post, *Acta Crystallogr.* **23**, 455 (1967).
- ¹⁶G. L. Paul and A. W. Pryor, *Acta Crystallogr. Sect. B* **27**, 2700 (1971).
- ¹⁷M. Balkanski, M. K. Teng, and M. Nusimovici, *Phys. Rev.* **176**, 1098 (1968).
- ¹⁸K. Akiyama, Y. Morioka, and I. Nakagawa, *J. Phys. Soc. Jpn.* **48**, 898 (1980).
- ¹⁹R. A. Noack and W. B. Holzapfel, in *High-Pressure Science and Technology*, edited by K. T. Timmerhaus and M. S. Barber (Plenum, New York, 1979).
- ²⁰D. M. Adams and S. K. Sharma, *J. Mol. Struct.* **71**, 121 (1981).
- ²¹K. L. Teo, Z. X. Shen, M. H. Kuok, and S. H. Tang, in *XIII International Conference on Raman Spectroscopy*, edited by W. Kiefer, M. Cardona, G. Schaack, F. W. Schneider, and H. W. Schrötter (Wiley, Chichester, 1992).
- ²²M. Md. Ibrahim, V. Ramachandran, K. Sarangapani, and R. Srinivasan, *J. Phys. Chem. Solids* **47**, 517 (1986).
- ²³R. M. Hazen and L. W. Finger, *J. Appl. Phys.* **50**, 6826 (1979).
- ²⁴H. Olijnyk, H. Däüfer, H.-J. Jodl, and H. D. Hochheimer, *J. Chem. Phys.* **88**, 4204 (1988); Ref. 45 therein.
- ²⁵R. M. Lynden-Bell, R. W. Impey, and M. L. Klein, *Chem. Phys.* **109**, 25 (1986).
- ²⁶G. F. Signorini, J.-L. Barrat, and M. L. Klein, *J. Chem. Phys.* **92**, 1294 (1990).
- ²⁷K. H. Hellwege, W. Lesch, M. Plihal, and G. Schaack, *Z. Phys.* **232**, 61 (1970).
- ²⁸K. S. Viswanathan, *Can. J. Phys.* **41**, 423 (1963).
- ²⁹D. Liu, F. G. Ullman, and J. R. Hardy, *Phys. Rev. B* **45**, 2142 (1992).
- ³⁰H. D. B. Jenkins and T. C. Waddington, *J. Inorg. Nucl. Chem.* **34**, 2465 (1972).
- ³¹F. Brehat and B. Wyncke, *J. Phys. C* **18**, 4247 (1985).